

Advanced Evaluation Algorithms for Standard and Dual Plane Particle Image Velocimetry

O. Ronneberger, M. Raffel, J. Kompenhans
DLR, Institut für Strömungsmechanik
Bunsenstr. 10, D-37073 Göttingen, Germany

ABSTRACT

The widely-used evaluation algorithms¹ for PIV recordings have some shortcomings, in that they introduce superfluous statistical and systematical errors. For example, they introduce the so-called “peak-locking” effect. These errors can be significantly reduced by using better algorithms.

The following considerably improved analysis and algorithms will be described and demonstrated on real PIV recordings:

- *Analysis of errors of CCD's and the electric transmission of the video signal.*
- *An FFT-based cross correlation algorithm using completely free-shaped and free-sized interrogation windows which exhibits the same accuracy as an optimally programmed direct correlation.*
- *A Gaussian fit algorithm using different weights for the values in the correlation plane due to the error distribution of correlation coefficients.*

1 INTRODUCTION

The major part of the PIV scientific community (including nearly all commercial PIV software vendors) is using the same evaluation algorithms for PIV recordings namely the cross correlation of two “power of 2” sized rectangular interrogation windows via FFT and the three-point peak fit estimator for sub pixel resolution, see, e.g., Willert and Gharib (1991); Westerweel (1993). These algorithms have the advantage that they are easy and fast to

¹These widely-used algorithms are the recording of the images with CCD cameras, the cross correlation of two “power of 2” sized rectangular interrogation windows via FFT and the three-point peak fit estimator for sub pixel resolution.

implement, but they introduce superfluous statistical and systematical errors.

Due to the increased requirements at our work on dual plane PIV (Raffel et al., 1995, 1996), where the height of the correlation peak is used to get information about the third component of the velocity, we had to consider all effects, that influence the shape, the height and the statistical and systematical errors of the correlation peak.

2 RECORDING OF THE IMAGES

There are three important effects influencing the shape of a particle image (Fig. 1). The influence of the particle size is negligible in nearly all our applications in air flows (e.g., the diameter of our oil droplets is around $1\mu m$). The geometrical image assuming an ideal camera objective is even smaller. Compared to the resolution of a CCD sensor (1 pixel is about $10\mu m \times 10\mu m$) we can neglect the particle diameter). So the geometrical particle image may be represented by a Dirac delta function.

As no camera objective is ideal, the real particle images on the image plane are distorted due to the limited spatial bandwidth of the camera objective (yielding the so-called Airy pattern) and due to aberrations (assumed to have Gaussian character). These two effects are combined in the point spread function of the camera objective. Usually only the effect of the aperture, the Airy pattern (Fourier transform of the circular aperture hole) is taken as the point spread function. In our experiments the effects of the lens aberrations were in the same order as the effects of the limited bandwidth. Especially near the borders of the image plane elliptical particle images are encountered frequently. However, if the point spread function does not change on the interrogation area, the light intensity distribution on the image plane can be mathematically described as the convolution of the geometrical

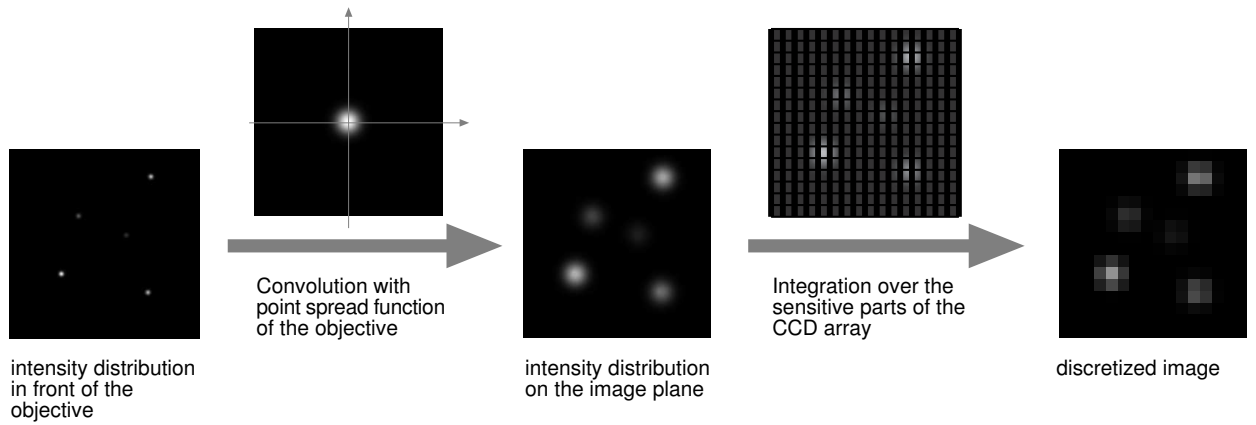


Fig. 1: Effects influencing the intensity distribution of a particle image.

particle images with the point spread function of the camera objective.

The next step is the integration of the light intensity over the sensitive area of each CCD pixel. In the case of a normal CCD sensor, the sensitivity is the same all over the active area of the pixel. Recent CCD sensors have micro lenses to collect more light. Then the sensitivity distribution for each pixel is a more complicated function. The integration over the sensitive area can mathematically be described as the convolution of the light intensity distribution on the image plane with the sensitivity function of the pixel and the sampling of this function at the centre of each pixel (see fig. 1).

After exposure the charges on the CCD are read out, amplified, and sequentially transmitted to the frame grabber as a time dependent voltage. The frame grabber is located in the camera or in the PC. The amplification and transmission may also introduce errors to the signal. Very common errors originate from an impedance mismatch between the amplifier, the transmission line and the frame grabber. A typical transmission error found with a digital camera (the frame grabber is located within the camera) is illustrated in Figure 2.

The image is transmitted as a sequence of horizontal lines, so the aforementioned effects are found only in the x direction. By comparing the joint probability of the values assumed by pixels succeeding in x - and y -direction respectively, one can detect such errors quite easily, since these statistics should be isotropic in a normal PIV recording. A more detailed discussion of these effects and an algorithm to correct such distorted images is described in Ronneberger (1998).

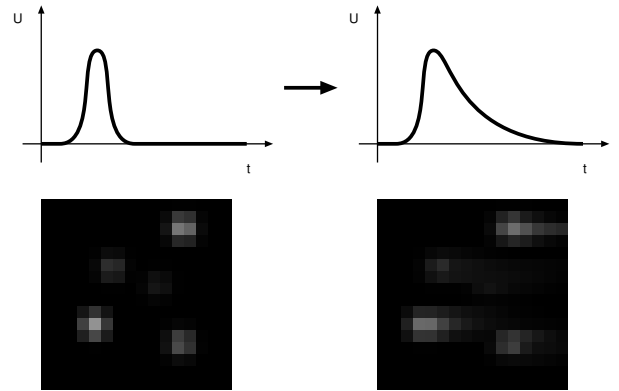


Fig. 2: Errors due to the electrical transmission of the video signal result in horizontal distortions of the image.

3 FFT-BASED FREE SHAPE CROSS CORRELATION

The estimate of the cross correlation is the central point of each PIV evaluation. The most common way to obtain an estimate is to take two equally-sized rectangular parts of the two PIV recordings (Fig. 3 and Fig. 4), and to make use of the FFT.

$$\mathbf{a}' := \mathbf{a} - \bar{\mathbf{a}} \quad (1)$$

$$\mathbf{b}' := \mathbf{b} - \bar{\mathbf{b}} \quad (2)$$

$$\mathbf{R} = \frac{\text{FFT}^{-1}(\text{FFT}^*(\mathbf{a}') \cdot \text{FFT}(\mathbf{b}'))}{\text{RMS}(\mathbf{a}') \cdot \text{RMS}(\mathbf{b}')} \quad (3)$$

The use of the standart FFT algorithm limits the possible linear dimensions of the partial images to powers of 2 (e.g., 16, 32, 64, 128, ...)

To understand the result of such an estimate of the correlation, the equivalent direct correlation is illustrated

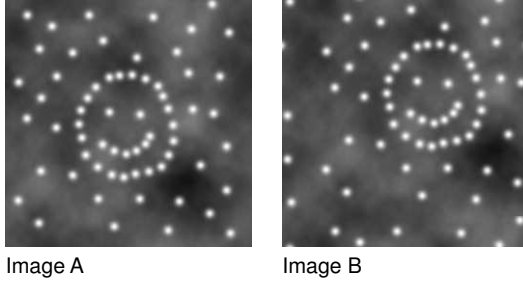


Fig. 3: Example for a pair of PIV recordings: The particle pattern has moved upwards and to the right

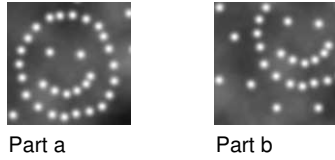


Fig. 4: The simplest estimate of the cross correlation, is based on two equally sized parts of the images. The parts are cut out at the same position in each image.

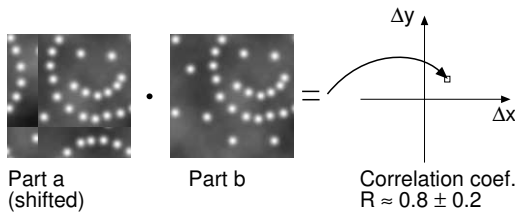


Fig. 5: The simple FFT-based correlation relies on the assumption that the partial images are parts of periodical images. So a shift of the partial image (a) results in the illustrated circular effects (i.e. the pixels leaving the image during the shift are wrapped around).

in Fig. 5 for one displacement $(\Delta x, \Delta y)$.

There are two effects that unnecessarily distort the correlation: Since the second partial image was taken at the same position as the first one, we did not capture all particle images of the shifted particle pattern. This is usually denoted as “in plane loss of pairs”. The second effect is a random contribution due to the decorrelation caused by the circular effects (in the illustrated example R varies between 0.6 and 1.0)

One common way to work around this problem is to cut the second partial image in a second pass at the proper position and calculate the cross correlation again. In this case, one obtains the undistorted correlation for at least one displacement. However, the neighbouring values in the correlation plane (which are used for the peak fit) are still distorted in the same way as above. This 2-pass method has some more shortcuts: It still relies on “power of 2” sized windows, and one has to define a rule to decide in the first pass, whether or not a found peak position is correct or represents an outlier.

The optimal accuracy is reached only if one cuts the proper part of the second image for *each* displacement. In this case the mean $(\bar{\mathbf{b}})$ and the RMS value $(\text{RMS}(\mathbf{b}'))$ depend on the displacement. It seems, that such an algorithm can only be implemented by calculating the correlation in a direct way:

$$R_{kl} = \frac{\sum_{i,j} (a_{ij} - \bar{\mathbf{a}}) \cdot (b_{i+k,j+l} - \overline{\mathbf{b}_{[k,l]}})}{\text{RMS}(\mathbf{a} - \bar{\mathbf{a}}) \cdot \text{RMS}(\mathbf{b}_{[k,l]} - \overline{\mathbf{b}_{[k,l]}})} \quad (4)$$

where $\mathbf{b}_{[k,l]}$ denotes the partial image \mathbf{b} cut at position k, l .

However, with some simple mathematical transformations eq. 4 can be evaluated using the FFT. The correlation coefficient of two datasets q and p (with subtracting the mean value) can be rewritten as

$$\sum_{i=1}^N (p_i - \bar{p}) \cdot (q_i - \bar{q}) = \sum_{i=1}^N p_i q_i - \frac{1}{N} \sum_{i=1}^N p_i \sum_{i=1}^N q_i \quad (5)$$

Therefore, we can postpone the subtraction of the mean value to a later stage of the calculation. Using eq. 5 we can rewrite the numerator of the direct correlation (Eq. 4) as

$$r_{kl} = \sum_{i,j} a_{ij} b_{i+k,j+l} - \frac{1}{NM} \sum_{i,j} a_{ij} \sum_{i,j} b_{i+k,j+l} \quad (6)$$

where $N \cdot M$ is the number of pixels in the partial image \mathbf{a} (the denominator will be treated in the same way). To use the FFT, we have to pad zeros around partial image \mathbf{a} to enlarge it to a “power of 2” size (Fig. 6). To get rid of the rectangular shape of the small window, we describe this cutting and padding procedure by multiplying with a

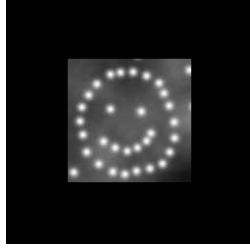


Fig. 6: To use free sized or even free shaped interrogation windows in an FFT-based correlation, the partial image must be padded with zeros to a “power of two” size

mask \mathbf{m} . The numerator of the direct correlation (Eq. 4) then becomes

$$r_{kl} = \sum_{i=1}^N \sum_{j=1}^M m_{ij} a_{ij} b_{i+k, j+l} - \frac{1}{\sum m_{ij}} \sum_{i=1}^N \sum_{j=1}^M m_{ij} a_{ij} \sum_{i=1}^N \sum_{j=1}^M m_{ij} b_{i+k, j+l} \quad (7)$$

With a normalized mask $\sum m_{ij} = 1$ we can now rewrite this equation utilizing the FFT as

$$\mathbf{r} = \text{FFT}^{-1} \left(\text{FFT}^*(\mathbf{ma}) \cdot \text{FFT}(\mathbf{b}) \right) - \sum \mathbf{ma} \cdot \text{FFT}^{-1} \left(\text{FFT}^*(\mathbf{m}) \cdot \text{FFT}(\mathbf{b}) \right) \quad (8)$$

Where \mathbf{ma} denotes the element by element multiplication of two images:

$$(\mathbf{ma})_{ij} = m_{ij} \cdot a_{ij} \quad (9)$$

With the definition of a cross correlation operator \otimes as

$$\mathbf{x} \otimes \mathbf{y} := \text{FFT}^{-1} \left(\text{FFT}^*(\mathbf{x}) \cdot \text{FFT}(\mathbf{y}) \right) \quad (10)$$

the completely free shaped cross correlation can be written as

$$\mathbf{R} = \frac{\mathbf{ma} \otimes \mathbf{b} - \sum \mathbf{ma} \cdot \mathbf{m} \otimes \mathbf{b}}{\sqrt{\left(\sum \mathbf{ma}^2 - (\sum \mathbf{ma})^2 \right) \cdot \left(\mathbf{m} \otimes \mathbf{b}^2 - (\mathbf{m} \otimes \mathbf{b})^2 \right)}} \quad (11)$$

The effect of such a correlation is illustrated in Fig. 7

In the standart cross correlation one has to compute three Fourier transforms. The FFT-based free shape correlation needs six Fourier transforms (The Fourier transform of the mask can be calculated once before the whole evaluation). So the computing time will only be doubled compared to the “traditional” evaluation. That is much faster

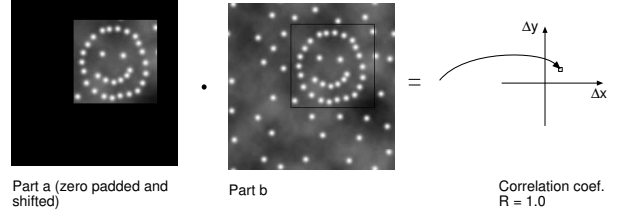


Fig. 7: The FFT-based free shape correlation combines the advantages of the direct correlation (free-sized and free-shaped windows, high accuracy) and the simple FFT-based correlation (high speed). The Figure shows the equivalent direct correlation for one displacement. Note: The mean and the variance of partial image (b) (used in the normalization of the correlation) must **not** be integrated over the whole partial image. Instead it has to be recalculated for each displacement. In the example shown above, the mean and variance are integrated only over the pixels inside the small rectangle. After a mathematical transformation of the governing equation it is still possible to make use of the FFT to reduce the computing time substantially.

than doing a direct correlation as described in Fincham and Spedding (1997). Please note, that this algorithm returns exactly the same result as the direct correlation described there. The only difference is, that it is much faster and more flexible with respect to the shape of the window.

4 THE STATISTICAL ERROR OF CORRELATION COEFFICIENTS

The error of a correlation coefficient depends on its value. It does not follow a normal distribution, which is obvious, because it can assume values only between -1 and 1. Accordingly the values in the correlation plane have to be weighted when the peak fit is performed.

For a correlation coefficient r of two datasets, where the distributions form a binormal or two-dimensional Gaussian distribution around their mean values, one can use *Fisher's z-transformation*, which associates each measured r with a corresponding z ,

$$z = \frac{1}{2} \ln \left(\frac{1+r}{1-r} \right) \quad (12)$$

Then, each z is approximately normally distributed with the same standard deviation. Although the grey values in a PIV recording are not really normally distributed, the Fisher transform still performs satisfactorily.

5 PEAK FITTING FOR SUB PIXEL RESOLUTION

To resolve the particle image displacement with sub pixel accuracy, usually a function is fitted to the correlation peak and its surroundings. According to section 2, the shape of the particle image is given by the point spread function of the camera objective convoluted with the sensitivity distribution of one CCD pixel. Assuming a Gaussian point spread function and a rectangular sensitivity distribution, the shape of the correlation peak will be a Gaussian bell convoluted with a 2D triangular function. Until now we have not found an analytical expression for this function. So we use a Gaussian bell, keeping in mind, that especially for very small particle images (diameter around 1 pixel) this assumption might produce some systematical and statistical errors.

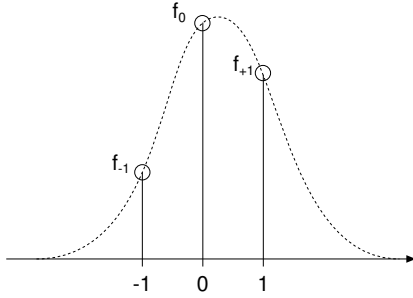


Fig. 8: The most common way to estimate the sub pixel position of the correlation peak is to use two one dimensional “fits” through the highest value and its two neighbours (three-point estimator). Although it is fast and easy to implement, it is only suitable for a very small range of particle image diameters and produces systematical errors for smaller peak diameters.

The most common method to fit the Gaussian curve to the correlation data, is to do two one dimensional fits to the highest value and its two neighbours (Fig. 8). A detailed analysis of these *three-point estimators* may be found in Westerweel (1993). Although the technique is fast and easy to implement, it is only suitable for a very small range of particle image diameters and produces systematical errors for smaller peak diameters. Particularly for elliptically shaped peaks (usually found in the corners of a PIV recording due to lens aberrations) the two one dimensional fits will not return the correct centre of this peak.

Therefore, we perform a two dimensional Gaussian fit using the Levenberg-Marquardt method from Press et al. (1992). Due to the aforementioned non-normal distribution of the errors of correlation coefficients, the best results would be reached, when fitting a Fisher-

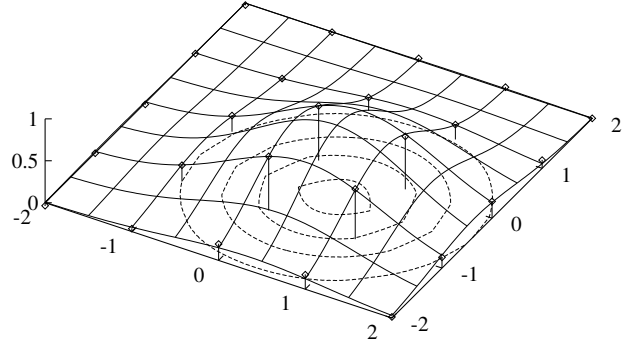


Fig. 9: Iterative Levenberg-Marquardt fit to determine the exact position of the correlation peak: A two dimensional Gaussian curve is fitted to the highest correlation coefficient and its surrounding in the correlation plane. This can handle elliptical peaks properly and the values can be weighted according to the Fisher transform.

transformed Gaussian bell to the Fisher-transformed correlation plane. As the Fisher-transformed Gaussian bell is a very unpractical and complicated function, we use the Fisher transform only to determine the weight for each value and perform a weighted fit (Fig. 9).

For very sharp peaks, all of the tested fitting algorithms tend to return too wide and too low Gaussian bells. With the assumption that all particle images inside the interrogation area have the same shape, due to the point spread function of the camera objective, all random correlation peaks will have the same shape as the main correlation peak, if there are not too big gradients of the particle displacement (Fig. 10).

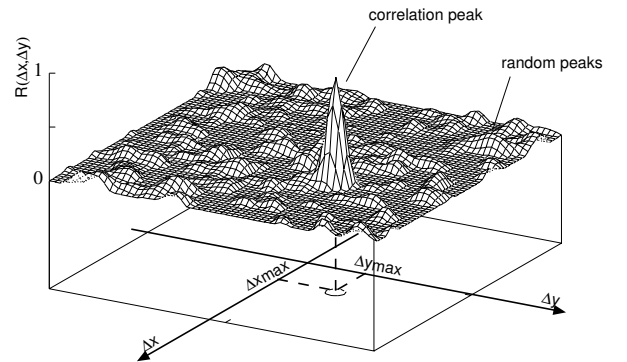


Fig. 10: All random peaks have the same shape as the correlation peak (assuming that all particle images inside the interrogation area had the same shape and that there are no big gradients of the particle displacement). This additional information can be used to achieve a better peak fit.

This additional information about the shape of the correlation peak can be extracted quite easily from the correlation function after eliminating the phase of the Fourier transform (see below). After the shape of the peak has been determined in this way, one can compute a peak fit with fixed shape parameters to determine the position and the height of the correlation peak.

This technique highly improves the quality of the peak fit (especially the determination of the peak height) and is the main key in the evaluation of dual plane recordings in air flows.

To determine the mean shape of all random correlation peaks, the phases in the Fourier transformed correlation function are eliminated by retaining only the magnitude of each spatial frequency component.

$$\mathbf{Q} = \text{FFT}^{-1} \left(\left| \text{FFT}(\mathbf{R}) \right| \right) \quad (13)$$

As a result of this operation, all random peaks are shifted to position (0,0) and one can perform a peak fit with a known position and height to determine the shape. Please note that this shift only works, if the peak shape is symmetrical and the real parts of the Fourier-transformed peak are positive. This is usually automatically fulfilled for correlation peaks of PIV recordings, because the shape of a particle image does not change from the first to the second recording. This results in a shifted auto correlation for the random peaks.

6 EXPERIMENTAL VERIFICATION OF THE IMPROVEMENTS

To quantify the improvements under real conditions, images with two 1024x1024 pixel CCD-cameras which looked through a beam splitter at the same measurement volume were taken at the same time. The non-moving air in the measurement volume was seeded with 1 μ m oil droplets and illuminated with an Nd:YAG-laser light sheet. Due to the small differences between the position, angle and magnification of the two cameras, an apparent displacement field results, that contains nearly all possible sub pixel displacements (Fig. 11). To determine the true displacement field, a matrix, describing a rotation, a magnification and a shift was fitted to the measured displacement field.

Prominent “peak-locking” effects are found, when the displacement field of these two images is evaluated by means of the usual three-point Gaussian fit. The RMS difference between this result and the true displacement field is 0.112 pixel. One can separate this error into a systematic error of 0.066 pixel and a statistical error of 0.087 pixel (figure 11).

The errors of the displacement field obtained with the improved techniques are shown in figure 13. The dis-

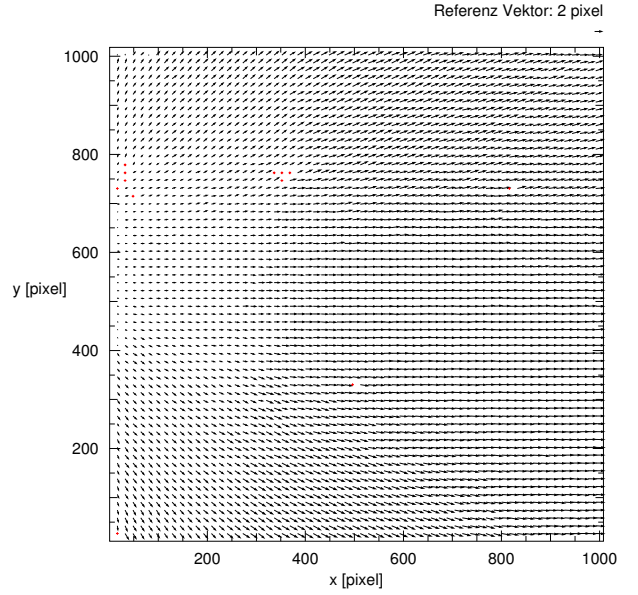


Fig. 11: The two images for this PIV evaluation were taken with two slightly misaligned cameras focused on the same part of non-moving air seeded with 1 μ m oil droplets.

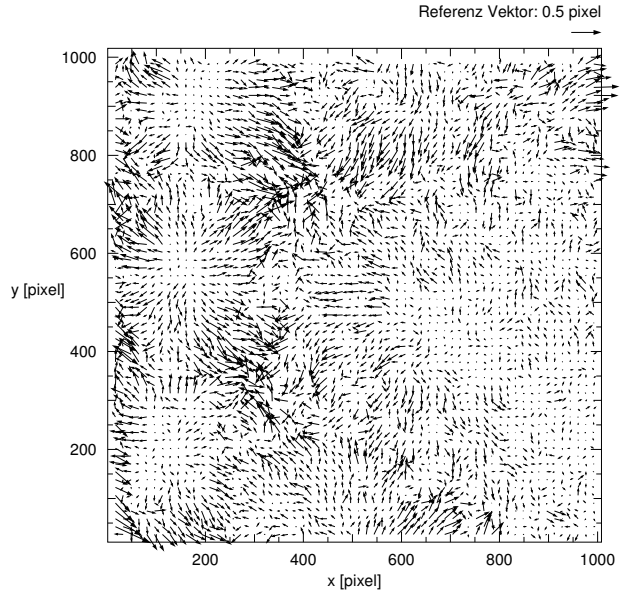


Fig. 12: Difference between the true displacement field and the measured displacement field using a normal 32x32 pixel interrogation window for the cross correlation and the three-point Gaussian fit to obtain the sub pixel position of the peak.

systematic error:	0.066 pixel
statistical error:	0.087 pixel
resulting error:	0.112 pixel

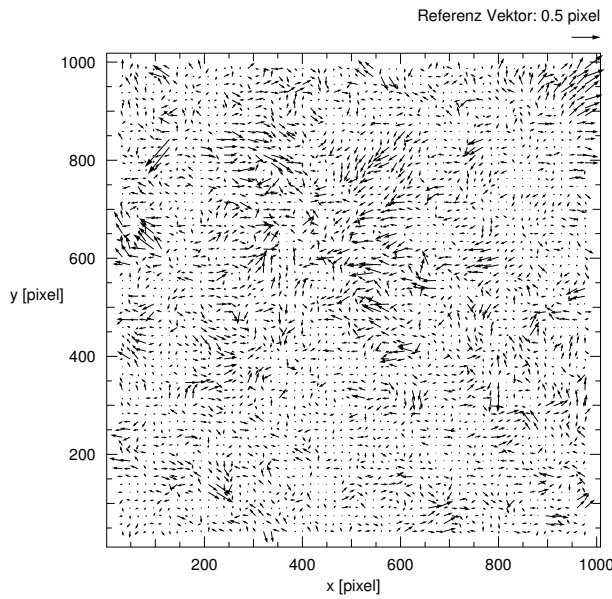


Fig. 13: Difference between the true displacement field and the measured displacement field using the advanced cross correlation with a 32x32 pixel interrogation window for the first and a 64x64 pixel interrogation window for the second image. The Gaussian peak fit was done using 9x9 pixels around the peak and the additional information from the random peaks.

systematic error:	0.0177 pixel
statistical error:	0.070 pixel
resulting error:	0.073 pixel

placements systematic error is reduced by nearly 75% to 0.0177 pixel and the statistical error is reduced by 20% to 0.070 pixel. The systematic and statistical error of the peak height is also reduced by 30% when using these techniques.

7 OTHER APPLICATIONS FOR THE FREE SHAPE CORRELATION

There are a lot of useful applications for the FFT-based free shape correlation. The first (and perhaps most important) advantage is that one can adapt the size of the interrogation window to the fluid dynamics of the experiment.

In regions with big gradients in one direction, e.g., a boundary layer which has big gradients normal to the wall, it can be useful to decrease the window size perpendicular to the wall while increasing it parallel to the wall.

Another application is the evaluation of stereo PIV recordings (using the Scheimpflug criteria) without de-warping the images before the evaluation. De-warping

of images can introduce errors to the shape of the particle images and it is very time consuming. It is now possible just to warp the interrogation grid and to warp the interrogation window shape.

In PIV recordings containing objects (e.g., a wing profile) one may now make a local adaption of the interrogation window shape, so that one can measure the boundary layer very close to curved wall of an object (Fig. 14 - 16)

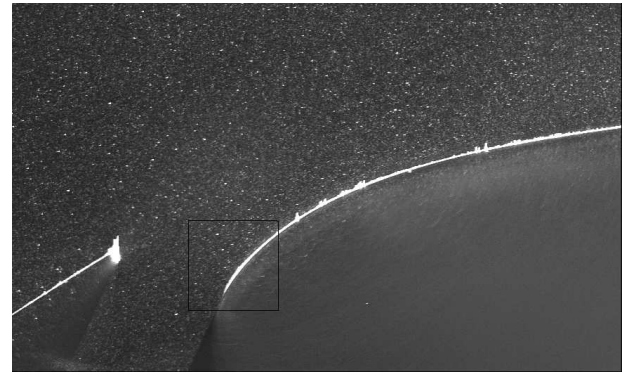


Fig. 14: PIV recording with curved walls and reflections

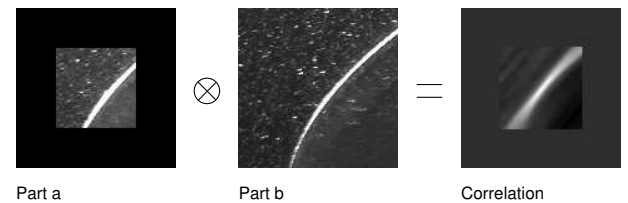


Fig. 15: With a rectangular interrogation window it is not possible to resolve the flow very close to the wing profile. The correlation plane contains no visible peak. (The operator \otimes denotes here the FFT-based free shape correlation)

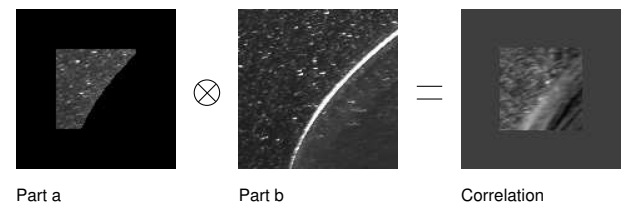


Fig. 16: With a free shaped interrogation window the flow close to the profile can be resolved. There is now a clear peak in the correlation plane near to the center

8 NOMENCLATURE

Two dimensional data arrays like images are represented by bold Roman letters (e.g., **a**). All operations on these arrays are defined element by element, e.g., $\mathbf{c} = \mathbf{a} \cdot \mathbf{b}$ has to be interpreted as $c_{ij} = a_{ij} \cdot b_{ij}$. The other definitions are:

$\bar{\mathbf{a}}$	Mean value of array a
$\text{RMS}(\mathbf{a})$	Variance of array a
$\text{FFT}(\mathbf{a})$	Fast Fourier transform of a
$\text{FFT}^{-1}(\mathbf{a})$	Reverse FFT
$\mathbf{a} \otimes \mathbf{b}$	simple FFT-based cross correlation of a and b
R	Array containing the normalized 2D correlation function

REFERENCES

- Fincham, A. M. & Spedding, G. R. 1997, Low cost, high resolution DPIV for measurement of turbulent fluid flow. *Experiments in Fluids*, vol 23, pp. 449–462.
- Press, W. H. et al. 1992, *Numerical recipes in C: the art of scientific computing – 2nd ed.* Cambridge University Press.
- Raffel, M., Derville, A., Willert, C., Ronneberger, O. & Kompenhans, J. 1996, Dual-plane correlation for three-dimensional particle image velocimetry on planar domains. In *8th International Symposium on Applications of Laser Techniques to Fluid Mechanics, Lisbon*.
- Raffel, M., Ronneberger, O., Gharib, M. & Kompenhans, J. 1995, Feasibility study of three-dimensional PIV by correlating images of particles within parallel light sheets. *Experiments in Fluids*, vol 19, pp. 69 – 77.
- Ronneberger, O. to appear 1998, Messung aller drei Geschwindigkeitskomponenten mit Hilfe der “particle image velocimetry” mittels einer Kamera und zweier paralleler Lichtschnitte. Forschungsbericht, Deutsches Zentrum für Luft- und Raumfahrt.
- Westerweel, J. 1993, *Digital particle image velocimetry: theory and application.* Delft University Press.
- Willert, C.E. & Gharib, M. 1991, Digital particle image velocimetry. *Experiments in Fluids*, vol 10, pp 181–193.